ChemComm

COMMUNICATION

View Article Online
View Journal | View Issue

Cite this: *Chem. Commun.*, 2025, **61**, 9964

Received 20th March 2025,
Accepted 23rd May 2025

DOI: 10.1039/d5cc01596k

rsc.li/chemcomm

Design and application of a non-toxic platinum derivative of the metal chelator Dp44mT for use as a long-term stable lysosome tracker†

Nandan Sheernaly,[a] Axel Steinbrueck,[a] Jasmine Ochs,[a] Frank Peeters,[b] Ronja Fiedler,[c] Franz Narberhaus,[c] Jacqueline Heinen-Weiler[d] and Nils Metzler-Nolte*[a]

The thiosemicarbazone Dp44mT and its Pt complex were conjugated to coumarin-based fluorophores. These conjugates proved to be versatile lysosome tracking agents. Specifically, Pt complex 5 remained trapped and produced reliable fluorescence emission in the lysosomes of HeLa cancer cells over 72 h, revealing its potential as a robust lysosome tracker.

Lysosomes, once referred to as "the suicide bags of cells," have been increasingly recognized for their role in various cellular processes.[1] In cancer cells, lysosomes support tumor progression by metabolizing macromolecules to supply energy and by releasing cathepsins that facilitate metastasis.[2] Furthermore, they are involved in triggering various programmed cell death mechanisms.[3] Hence, labeling lysosomes and studying their cellular dynamics is beneficial for understanding the progression of cancer and developing new therapeutics.[4] To this end, we envisioned developing new lysosome-localizing fluorescent agents to serve as versatile tools for theranostics.

Di-2-pyridylketone-4,4-dimethyl-3-thiosemicarbazone (Dp44mT) is a promising anti-cancer agent that is known to localize in the lysosomes. It belongs to the di-2-pyridyl-thiosemicarbazone (DpT) class of chelators (Fig. 1).[5] DpTs enter the lysosome using P-glycoprotein (Pgp) and preferentially bind Cu(II) and Fe(II) ions to form redox active complexes that generate reactive oxygen species (ROS).[6,7] The generated ROS causes lysosomal membrane permeabilization (LMP), eventually leading to apoptosis.[7] Due to their unique mode of action, DpTs have shown strong antiproliferative activities both *in vitro* and *in vivo*. However, their clinical development has been limited by side effects. Dp44mT caused cardiac fibrosis in murine xenograft models of lung carcinoma at higher doses, and DpC has not advanced beyond Phase I clinical trials (NCT02688101).[5,8] Herein, we took advantage of Dp44mT's preference for lysosomal localization and synthesized a fluorophore conjugate of Dp44mT to target lysosomes. Besides, this conjugate serves to provide direct visual proof of Dp44mT's ability to localize in lysosomes, addressing the limitations of previous studies that relied on indirect evidence, such as the dispersion of cathepsin D.[7]

Apart from Cu(II) and Fe(II), DpTs have demonstrated excellent metal-binding properties, chelating various transition metal ions. Previous research has shown that DpT-metal complexes only exert significant cytotoxicity after transmetallation with Cu(II).[9] Considering this, we selected Pt(II) to synthesize an inert metal complex of the fluorophore conjugate with applications as a lysosome tracker for long-term incubations. While Pt complexes have been reported to show lysosomal localization,[10] this is, to the best of our knowledge, the first instance of a thiosemicarbazone-based metal complex with lysosomal specificity. We describe the synthesis of these fluorophore conjugates, explore their cytotoxic activity, and investigate their ability to target lysosomes using confocal microscopy.

The choice of the fluorophore is critical for the synthesis of fluorophore conjugates. The fluorophore's excitation and emission

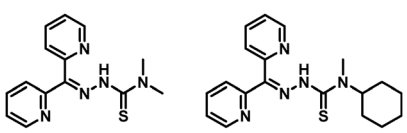

Fig. 1 Structures of representative DpTs.[5]

[a] *Faculty of Chemistry and Biochemistry, Inorganic Chemistry I – Bioinorganic Chemistry, Ruhr-University Bochum, Universitätsstrasse 150, 44780 Bochum, Germany. E-mail: nils.metzler-nolte@rub.de*
[b] *Applied Microbiology, Faculty of Biology and Biotechnology, Ruhr-University Bochum, Universitätsstrasse 150, 44780 Bochum, Germany*
[c] *Microbial Biology, Faculty of Biology and Biotechnology, Ruhr-University Bochum, Universitätsstrasse 150, 44780 Bochum, Germany*
[d] *Medical Imaging Center (MIC), Electron Microscopy Medical Analysis – Core Facility (EMMA^{CF}) Faculty of Medicine, Ruhr-University Bochum, Universitätsstrasse 150, 44780 Bochum, Germany*

† Electronic supplementary information (ESI) available. CCDC 2427619. For ESI and crystallographic data in CIF or other electronic format see DOI: https://doi.org/10.1039/d5cc01596k

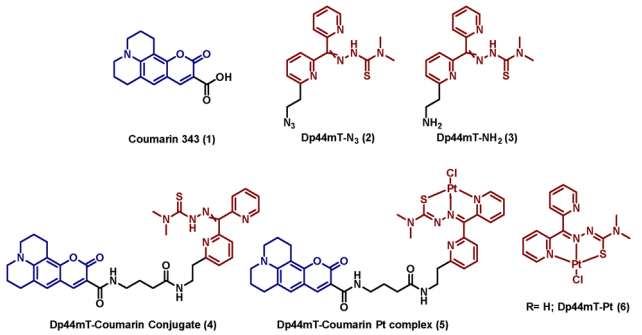

Fig. 2 Fragments **1–3** were used to synthesize the Dp44mT-coumarin conjugate **4** and the corresponding Pt(II) complex **5**. The Pt(II) complex of Dp44mT **6** served as control.

spectra need to be well-separated from those of the organelle tracker used during colocalization studies to ensure minimal cross-talk between channels. To this end, we selected coumarin 343 (**1**, $\lambda_{exc}/\lambda_{em}$: 443/462 nm) to synthesize conjugates **4** and **5** (Fig. 2).

The synthesis of the fluorophore conjugates commenced by equipping Dp44mT with an azide functionality **2**, which was obtained as a 1 : 1 mixture of *E*/*Z* isomers following our previously reported synthetic route.[11] Initial attempts at performing the conjugation *via* azide–alkyne 'click' chemistry were unsuccessful and will not be further detailed here. Consequently, **2** was reduced to the corresponding primary amine **3** using the Staudinger reaction. This allowed the conjugation of Dp44mT to **1** through standard peptide coupling conditions, affording **4** in 65% yield as a mixture of *E*/*Z* isomers, which was deduced by the presence of twice the number of signals in the ^{1}H NMR spectrum (Fig. S7, ESI†). The ligand was then treated with K_2PtCl_4 to procure the desired Pt complex **5** (see ESI† for detailed schemes and characterization data). The disappearance of the peak at ~15 ppm, which corresponds to the hydrazidenyl –NH in the ^{1}H NMR spectrum of **4**, was the first indication of successful complex formation. Furthermore, **5** was obtained as a single diastereomer, as indicated by the ^{1}H NMR spectrum (Fig. S11, ESI†), which contained a single set of signals, unlike **4**. We hypothesized that *E*/*Z* isomer interconversion occurred due to rotation about the N–N bond during complexation.

Attempts to crystallize complex **5** were unsuccessful. As a surrogate, we synthesized the corresponding Pt complex of parent Dp44mT **6** to gain insights into the geometry of **5**. Single crystals of **6** were obtained by slow diffusion of hexane into an acetonitrile solution of the metal complex and analyzed *via* X-ray diffraction (Fig. S19 and Table S1, ESI†). The results confirmed that Dp44mT formed complexes of 1 : 1 stoichiometry with Pt(II). The complex crystallized in the monoclinic space group, adopting a distorted square planar geometry with N1-Pt1-N3 and N3-Pt1-S1 bond angles measured at ~81° and ~85° respectively, consistent with analogous Pt(II) complexes.[12,13] Moreover, the C–S bond distance was 1.75 Å. This is longer than a typical C–S bond in thiosemicarbazones (1.68 Å), suggesting that the ligand had tautomerized during complexation.[14]

After confirming the stability of compounds **4**, **5**, and **6** in DMSO-d_6 over 24 h using NMR spectroscopy (Fig. S20–S22, ESI†), we investigated their stability in cell culture medium over 3 days at room temperature using UV/Vis spectroscopy (Fig. S23, ESI†). For reference, we recorded the UV/Vis absorption spectrum of the compounds in water, measured immediately after dissolution (Fig. S24, ESI†). Gratifyingly, the absorption profiles of the compounds in water were similar to those in cell culture medium, with no significant differences observed. Moreover, the absorption profiles of all compounds remained unchanged over time in cell culture medium, suggesting their structural integrity was maintained throughout the incubation period.

As mentioned before, the *in vitro* activity of DpT metal complexes reportedly depends on the complex's stability in the presence of Cu(II) both within lysosomes (pH 5) and extracellular conditions (pH 7.4). To evaluate this, we treated aqueous solutions of **5** and **6** in acetate buffer (pH 5, 100 mM) with 5.0 equiv. of $CuCl_2$ and monitored for changes over 24 h in the UV/Vis absorption profile (Fig. S25, ESI†). The experiment was repeated in cell culture medium (Fig. S26, ESI†). Gratifyingly, both Pt complexes remained stable under both conditions, indicating their robustness in lysosomal and physiological environments.

With the conjugates characterized, we moved on to investigate their antiproliferative activities against HeLa cells using a standard MTT assay. As summarized in Table 1, conjugating Dp44mT to fluorophores was detrimental to its potency, with **4** being approximately 100-fold less cytotoxic (IC_{50} = 800 ± 100 nM) compared to the parent molecule Dp44mT (IC_{50} = 9.0 ± 0.3 nM). In line with design expectations, metal complexation had an impact on the potency of **4**, as the IC_{50} value of **5** was significantly lower than that of the ligand at 58.2 ± 4.3 μM after 72 h incubation. The Pt complex of Dp44mT **6**, used as a control, also demonstrated to be approximately 200-fold less potent than Dp44mT. Furthermore, none of the conjugates suppressed cell viability after 24 h incubation, even at the highest tested concentration (15 μM), suggesting their potential as cellular probes for extended incubation. Similarly, the parent Dp44mT also did not suppress cellular viability within 24 h, which is consistent with previous findings.[15]

Before observing the behavior of the compounds in cells using confocal microscopy, we measured the fluorescence excitation and emission spectra at 10 μM for each compound in water (Fig. S29, ESI†). Upon excitation at 450 nm, the compounds showed similar emission properties with λ_{max} at 492 nm. Notably, the metal complex **5** demonstrated a 7–8-fold decrease in fluorescence intensity compared to the ligand, indicating a quenching effect caused by metal complexation.

Table 1 *In vitro* activity of compounds **4–6** displayed as IC_{50} (μM) values determined by MTT assay. HeLa cells were incubated with the respective compounds for the indicated time period using Dp44mT as positive control and 0.5% DMSO as negative control. The values are presented as the mean of three independent experiments ± standard deviation. The individual dose–response curves are in the ESI (Fig. S27 and S28)

IC_{50} (μM)		
Compound	24 h	72 h
Dp44mT	>15	0.009 ± 0.0003
4	>15	0.8 ± 0.1
5	>15	58.2 ± 4.3
6	>15	1.9 ± 0.2

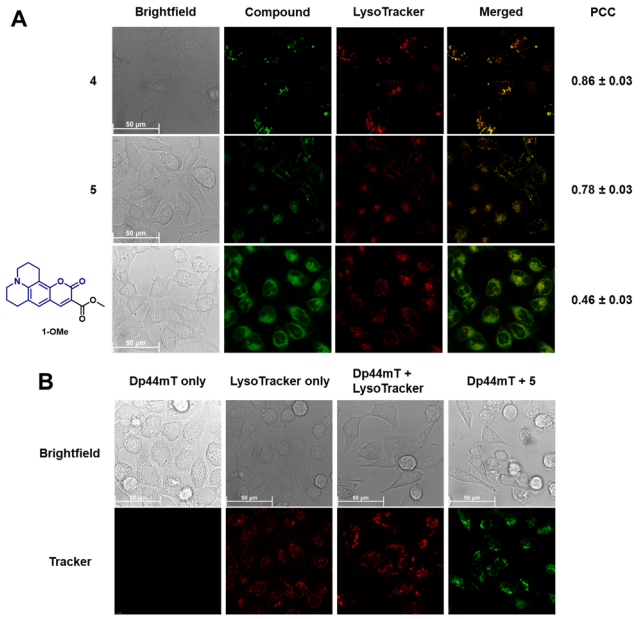

Fig. 3 (A) Live-cell images acquired after incubating HeLa cells with for 24 h compounds **4**, **5**, or the control **1-OMe** at 10 μM, respectively. The green channel shows the respective compound, and the red channel LysoTracker deep red. The merged channels and the corresponding Pearson Correlation Coefficients (PCC) ± standard deviation are provided on the right. (B) Control live-cell images captured after incubating HeLa cells with only parent chelator Dp44mT for 24 h, only LysoTracker, coincubation of Dp44mT and LysoTracker and, Dp44mT with Pt-conjugate **5**. Control images without tracker coincubation are in the ESI† (Fig. S30), as well as further experimental details and enlarged versions of these images (Fig. S32 and S33, ESI†).

This was confirmed by measuring the quantum yield of **4** (0.059) and **5** (0.008) relative to coumarin-343 **1** in water. Nonetheless, the photophysical properties of the compounds allowed their visualization and sub-cellular localization patterns using confocal microscopy.

HeLa cells were incubated with the respective conjugates (10 μM) and observed under a confocal microscope. We used the methyl ester of **1**, namely **1-OMe**, as control (10 μM). After 6 h of incubation (Fig. S30 and S31, ESI†), **1-OMe** appeared dispersed throughout the cytoplasm. In contrast, we observed that the fluorescence from conjugate **4** and its Pt complex **5** punctuated as specks throughout the cytoplasm. These results indicated that the tethered Dp44mT and the Pt complex dictated the localization of the conjugates, respectively.

Further, we performed colocalization experiments for **4** and **5** with a commercial lysosome tracking dye (LysoTracker™ Deep Red) to confirm their localization in lysosomes. Additionally, we compared incubation times of 6 h and 24 h to identify potential changes in the localization patterns (Fig. 3A and Fig. S31, ESI†). Expectedly, both the ligand and its Pt complex demonstrated excellent colocalization with the Lysotracker. While there was an observable increase in colocalization after 24 h relative to the 6 h time point for both conjugates, the effect was more pronounced in the case of **4**, where the corresponding Pearson correlation coefficient (PCC) increased from 0.63 to 0.86. These findings confirm Dp44mT's preference for lysosomal localization, which is consistent with previous studies.[7] Notably, these results are in good agreement with the slow mode of action of Dp44mT's cytotoxic effect on cells, as observed in prior MTT assays. Additionally, we inferred that complexing Pt to Dp44mT did not hamper its lysosomal directing ability, as the Pt complex also localized in lysosomes.

To further validate that **4** localized in lysosomes, we incubated parent Dp44mT for 24 h and colocalized it with LysoTracker (Fig. 3B). Interestingly, we observed the formation of large fluorescent spots in the colocalized sample, similar to those formed with **4**, and not when the LysoTracker was incubated independently. These findings suggest that the presence of Dp44mT induces lysosomal swelling over time. Since swollen lysosomes are susceptible to LMP,[16,17] these results further corroborate previous studies that suggest lysosomal accumulation and permeabilization as one of Dp44mT's modes of action.[7] The lysosomal swelling upon incubating HeLa cells with **4** for 24 h was further verified using ultrastructural transmission electron microscopy (TEM). As shown in Fig. S36 (ESI†) (black arrows), treatment with **4** resulted in a 200% increase in lysosomal size compared to the untreated control (Fig. 4). Furthermore, consistent with previous studies with analogous DpTs,[18] the mitochondria, identifiable by their cristae structure, also appeared rounded and swollen, indicating mitochondrial damage.

In contrast, lysosomal swelling was not observed after 24 h in the case of the Pt complex **5**, suggesting that the typical mode of action expected for Dp44mT is not engaged at this time point. This result is in good agreement with the observed low *in vitro* cytotoxicity. Moreover, the observation suggests that the Pt complex remained stable within the cell, as decomplexation would have resulted in lysosomal swelling. As shown in Fig. 3B, co-incubation of Dp44mT and **5** led to enlarged lysosomes, similar to Dp44mt + LysoTracker, further attesting to its preference for the lysosome. Hence, the presence of an unobstructed metal binding site is required for Dp44mT to cause lysosomal swelling and exert its anti-cancer activity.

Subsequently, to confirm the presence of Pt in lysosomes, we incubated **5** with HeLa cells for 24 h and used a commercial lysosome extraction kit to extract the organelle. The metal content was then analyzed using inductively coupled plasma mass spectrometry (ICP-MS). As illustrated in Fig. S37 (ESI†), a significant concentration of Pt was found in the lysosomes

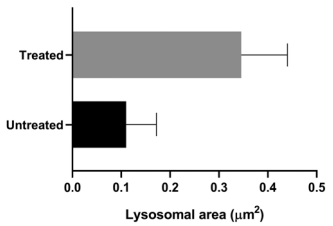

Fig. 4 Comparing the area of lysosomes measured after TEM analysis of untreated (control) and **4** treated HeLa cells. See ESI† for further experimental details.

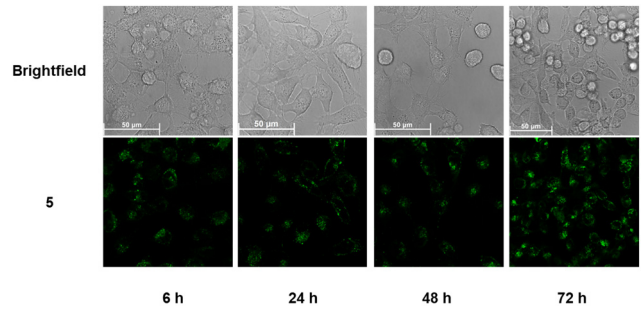

Fig. 5 Live-cell images of HeLa cells after incubating with **5** for 6, 24, 48, and 72 h, respectively. Enlarged images have been included in the ESI† (Fig. S35).

(~51 ng mg^{-1} of protein). This finding not only proves the uptake of the Pt(II) complex **5** into cells but also corroborates its strong accumulation and stability within lysosomes.

Taken together, both **4** and **5** can be used as lysosome trackers for different purposes. **4**'s ability to enlarge lysosomes over 24 h makes it suitable for labeling and highlighting this organelle. Additionally, the potent *in vitro* activity of the conjugated Dp44mT makes it an excellent theranostic agent. In contrast, **5**'s inertness allows for its use as a robust lysosome tracker for long-term studies.

To further investigate the behavior of the conjugates in cells, we extended the incubations of **4** and **5** to 48 h and 72 h and observed the effects on cells using confocal microscopy. In the case of **4** (Fig. S34, ESI†), while most cells were dead after 48 h, those that had survived continued to exhibit swollen lysosomes. However, unlike at the 24 h time point, some fluorescence had begun spilling into the cytoplasm, indicating that the lysosomal membrane had indeed been permeabilized. By 72 h, a substantial amount of **4** appeared to have escaped the lysosomes and was distributed throughout the cytoplasm of severely stressed cells. On the other hand, the Pt complex appeared harmless to the cells as it remained trapped in lysosomes even after 72 h (Fig. 5).

In summary, we have rationally designed and synthesized two new lysosome trackers by leveraging thiosemicarbazone Dp44mT's lysosome-directing ability. Dp44mT was conjugated to the fluorophore coumarin and complexed with Pt(II) to suppress the ligand's *in vitro* activity. As envisioned, the IC_{50} values of the complexes were significantly higher than that of the ligand (75-fold). Subsequently, localization patterns of the conjugates were investigated using confocal microscopy. The Dp44mT-coumarin conjugate accumulated in lysosomes, with its PCC with the LysoTracker increasing over time, indicating gradual accumulation. Enlarged lysosomes were observed after 24 h, which showed signs of permeabilization after 48 h, providing further insights regarding the mechanism of action of Dp44mT against cancer cells. Based on these results, we believe that the conjugate can be used as an effective tool for theranostics as it combines the fluorescent properties of coumarin with the potent antiproliferative activity of Dp44mT. Contrastingly, although the Pt complex localized in the lysosome, it did not induce swelling, remaining stable over several days confined in the organelle. This indicates its potential as a stable lysosome tracker for long-term incubations. Further studies in our lab will expand on the metal-driven effects of such complexes while delving into their mechanism of action in cells.

We are grateful to Prof. Dr Stephan Hahn (Ruhr-University Bochum, Molecular gastroenterological oncology) for assisting with protein quantification. N. S. thanks the Fonds der Chemischen Industrie for a PhD fellowship. A. S. thanks the Deutsche Forschungsgemeinschaft DFG (STE 3245/1-1, grant no. 518777768). J. O., F. P., F. N., and N. M.-N. acknowledge the DFG-funded RTG 2341 "MiCon" for financial support.

Data availability

The data supporting the findings of this study are available within the article and its ESI.†

Conflicts of interest

There are no conflicts to declare.

References

1 Z. Zhang, P. Yue, T. Lu, Y. Wang, Y. Wei and X. Wei, *J. Hematol. Oncol.*, 2021, **14**, 79.
2 T. Tang, Z. Yang, D. Wang, X. Yang, J. Wang, L. Li, Q. Wen, L. Gao, X. Bian and S. Yu, *Cell Biosci.*, 2020, **10**, 131.
3 N. Kavčič, K. Pegan and B. Turk, *Biol. Chem.*, 2017, **398**, 289–301.
4 D. C. Barral, L. Staiano, C. Guimas Almeida, D. F. Cutler, E. R. Eden, C. E. Futter, A. Galione, A. R. A. Marques, D. L. Medina, G. Napolitano, C. Settembre, O. V. Vieira, J. M. F. G. Aerts, P. Atakpa-Adaji, G. Bruno, A. Capuozzo, E. De Leonibus, C. Di Malta, C. Escrevente, A. Esposito, P. Grumati, M. J. Hall, R. O. Teodoro, S. S. Lopes, J. P. Luzio, J. Monfregola, S. Montefusco, F. M. Platt, R. Polishchuck, M. De Risi, I. Sambri, C. Soldati and M. C. Seabra, *Traffic*, 2022, **23**, 238–269.
5 P. Heffeter, V. F. S. Pape, É. A. Enyedy, B. K. Keppler, G. Szakacs and C. R. Kowol, *Antioxid. Redox Signaling*, 2019, **30**, 1062–1082.
6 P. J. Jansson, T. Yamagishi, A. Arvind, N. Seebacher, E. Gutierrez, A. Stacy, S. Maleki, D. Sharp, S. Sahni and D. R. Richardson, *J. Biol. Chem.*, 2015, **290**, 9588–9603.
7 D. B. Lovejoy, P. J. Jansson, U. T. Brunk, J. Wong, P. Ponka and D. R. Richardson, *Cancer Res.*, 2011, **71**, 5871–5880.
8 M. Whitnall, J. Howard, P. Ponka and D. R. Richardson, *Proc. Natl. Acad. Sci. U. S. A.*, 2006, **103**, 14901–14906.
9 M. Dharmasivam, B. Kaya, T. P. Wijesinghe, V. Richardson, J. R. Harmer, M. A. Gonzalvez, W. Lewis, M. G. Azad, P. V. Bernhardt and D. R. Richardson, *Chem. Sci.*, 2024, **15**, 974–990.
10 V. Ramu, P. Kundu, A. Upadhyay, P. Kondaiah and A. R. Chakravarty, *Eur. J. Inorg. Chem.*, 2021, 831–839.
11 N. Sheernaly, I. Shajan, A. Steinbrueck, B. Albada and N. Metzler-Nolte, *RSC Med. Chem.*, 2025, DOI: 10.1039/d5md00154d.
12 E. Bermejo, R. Carballo, A. Castiñeiras, R. Domínguez, A. E. Liberta, C. Maichle-Mössmer, M. M. Salberg and D. X. West, *Eur. J. Inorg. Chem.*, 1999, 965–973.
13 R. Salehi, S. Abyar, F. Ramazani, A. A. Khandar, S. A. Hosseini-Yazdi, J. M. White, M. Edalati, H. Kahroba and M. Talebi, *Sci. Rep.*, 2022, **12**, 8316.
14 R. Restivo and G. J. Palenik, *Acta Crystallogr., Sect. B*, 1970, **26**, 1397–1402.
15 M. Krchniakova, S. Paukovcekova, P. Chlapek, J. Neradil, J. Skoda and R. Veselska, *Front. Pharmacol.*, 2022, **13**, 976955.
16 G. Kroemer and M. Jäättelä, *Nat. Rev. Cancer*, 2005, **5**, 886–897.
17 F. Wang, R. Gómez-Sintes and P. Boya, *Traffic*, 2018, **19**, 918–931.
18 S. Hager, K. Korbula, B. Bielec, M. Grusch, C. Pirker, M. Schosserer, L. Liendl, M. Lang, J. Grillari, K. Nowikovsky, V. F. S. Pape, T. Mohr, G. Szakács, B. K. Keppler, W. Berger, C. R. Kowol and P. Heffeter, *Cell Death Dis.*, 2018, **9**, 1052.